Anisotropy of electronic lifetime in indium

Bijan K. Bhattacharyya* and James C. Swihart
Department of Physics, Indiana University, Bloomington, Indiana 47405
(Received 13 October 1983; revised manuscript received 30 April 1984)

Electronic lifetimes limited by the electron-phonon interaction are calculated on both the second- and third-zone Fermi surfaces in indium for temperatures 0.1—10 K. Pseudopotential models for the true Fermi surface, electronic band velocity, many-OPW (orthogonalized plane wave) electronic wave function, phonon spectra, and the electron-phonon interaction are used in this calculation. The electron-phonon matrix elements are evaluated by a Monte Carlo method, and the inverse lifetime $\tau^{-1}(\vec{k})$ is calculated in terms of the Eliashberg function $\alpha^2F(\vec{k},\omega)$. T^3 behavior of $\tau^{-1}(\vec{k})$ is obtained only on free-electron-like regions and at low temperatures, as expected. Deviation from the T^3 dependence is found near the ridges of the Fermi surface. A huge anisotropy (30:1 at 3 K) in $\gamma(\vec{k})$, the T^3 coefficient of $\tau^{-1}(\vec{k})$, is found over the second-zone surface, with minimum values on the free-electron-like regions and maximum values on the ridges. Quantitative agreement with experiment for $\gamma(\vec{k})$ in the [111] direction on the second-zone surface (a free-electron-like region) is obtained. Good agreement is also found for the orbit-averaged scattering rate at 4 K with the experiments of Hoff *et al.* However, our local scattering rate is more peaked with larger values on the ridges of the second-zone surface than the local values extracted by Hoff *et al.* from their orbit-averaged results by an inversion scheme, indicating that their inversion scheme is not correct. Our orbit-averaged results on the third-zone surface are not in as good agreement with the experiments of Hoff *et al.* (differing by as much as 20—40%) as are the results on the second-zone surface.

I. INTRODUCTION

The scattering rate or inverse lifetime $\tau^{-1}(\vec{k})$ of the electron quasiparticles near the Fermi surface in a metal at low temperatures is a very sensitive probe of the electron-phonon interaction. The most extensive precise lifetime measurements ever carried out for a polyvalent metal have been done on indium,[1-7] and an anisotropy in excess of 20:1 has been claimed. However, no calculations have been performed for this metal to see if the electron-phonon interaction using a pseudopotential can account for these results in a quantitative way. In this paper we are concerned with a detailed calculation of $\tau^{-1}(\vec{k})$ point by point on the Fermi surface as obtained from the anisotropic Eliashberg function $\alpha^2F(\vec{k},\omega)$. We are also concerned with explaining the surprising results of Hoff *et al.*[1-3] in which with the inversion of their orbit-averaged data they find maxima or near maxima for τ^{-1} on the second-zone hole surface in the [100] and [001] directions which are free-electron-like regions.

A simple model for the inverse lifetime predicts a T^3 behavior at least for low temperatures and in free-electron-like regions. Traditionally, therefore, the anisotropy is characterized by $\gamma(\vec{k})$ which is just the T^3 coefficient of $\tau^{-1}(\vec{k})$ given by

$$\gamma(\vec{k})=\tau^{-1}(\vec{k})/T^3 . \quad (1)$$

With this definition, $\gamma(\vec{k})$ may depend on temperature.

The theory of the electron lifetime limited by the electron-phonon interaction is discussed in Sec. II where some analytical results are reviewed. $\tau^{-1}(\vec{k})$ is very sensitive to the contribution at low energy of the electron-phonon interaction, at least for low temperatures. A relatively accurate numerical calculation of the low-ω part of the anisotropic function $\alpha^2F(\vec{k},\omega)$ is thus needed to achieve reliable results. This is emphasized in Sec. III where we discuss the numerical methods of calculating both the local value $\tau^{-1}(\vec{k})$ and orbit-averaged value $\bar{\tau}^{-1}$ using a Monte Carlo method.

Experimentally, the scattering rate or inverse lifetime can be measured by a variety of experimental methods, namely, radio frequency size effect (RFSE), Azbel'-Kaner cyclotron resonance (AKCR), and surface Landau-level resonance (SLLR) experiments. While both RFSE and AKCR experiments (for parallel field geometry; i.e., both $\vec{E}$ and $\vec{H}$ parallel to the sample surface) measure the scattering rate averaged over extremal cyclotron orbits, SLLR experiments probe local values of the rate on the Fermi surface. (The local rate can also be obtained from the limiting-point RFSE and AKCR experiments for a magnetic field orientation tilted with respect to the sample surface.) Measurements of lifetimes in indium have been done by all three methods. Extensive RFSE measurements on both the second- and third-zone surfaces for the orbit-averaged lifetime have been performed by Hoff and co-workers.[1-3] Castaing and Goy[4] have reported their results of AKCR measurements for a third-zone orbit. Limiting-point RFSE measurements for a few local values of inverse lifetime have also been obtained by Snyder[5] and Krylov and Gantmakher.[6] So far SLLR measurements have been done only for one direction on the second-zone [110] orbit by Doezma and Koch.[7]

Results of our calculations for lifetimes are presented in

Sec. IV for the second-zone surfaces and in Sec. V for the third-zone surfaces. Comparison with experiments is also made. Finally the conclusion is presented in Sec. VI.

II. THEORY OF ELECTRON LIFETIME

The inverse lifetime $\tau^{-1}(\vec{k})$ or scattering rate of individual electron quasiparticles on the Fermi surface by phonon emission or absorption is related to the Eliashberg function $\alpha^2F(\vec{k},\omega)$ and is given by[8]

$$\tau_b^{-1}(\vec{k},T)=4\pi\int_0^\infty d\omega\frac{\alpha^2F(\vec{k},\omega)}{\sinh(\omega/k_BT)}\ , \tag{2}$$

which goes to 0 at zero temperature. The anisotropic function $\alpha^2F(\vec{k},\omega)$ in Eq. (2) is a measure of the scattering from electron state $\vec{k}$:

$$\alpha^2F(\vec{k},\omega)=\frac{1}{(2\pi)^3}\int_{FS}\frac{dS'}{v_b(\vec{k}')}\times\sum_\sigma|g_{\vec{k}\vec{k}'\sigma}|^2\delta(\omega-\omega_{\vec{q}\sigma})\ , \tag{3}$$

where the integral is over the Fermi surface, $v_b(\vec{k}')$ is the band velocity at $\vec{k}'$, and $\omega_{\vec{q}\sigma}$ is the phonon frequency of wave vector $\vec{q}$ and polarization vector $\hat{e}_{\vec{q}\sigma}$. $\vec{q}$ is related to $\vec{k}$ and $\vec{k}'$ through the conservation rule

$$\vec{q}=\vec{k}-\vec{k}'-\vec{G}\ , \tag{4}$$

where $\vec{G}$ is the reciprocal-lattice vector which brings $\vec{q}$ to the first Brillouin zone. For normal-scattering processes $\vec{G}=\vec{0}$ and for umklapp-scattering processes $\vec{G}\neq\vec{0}$. The electron-phonon matrix element in the local-pseudopotential approximation is given by[9]

$$g_{\vec{k}\vec{k}'\sigma}=-i(2MN\omega_{\vec{q}\sigma})^{-1/2}\sum_{\vec{G},\vec{G}'}a_{\vec{G}}(\vec{k})a^*_{\vec{G}'}(\vec{k}')(\vec{k}'-\vec{G}'-\vec{k}+\vec{G})\cdot\hat{e}_{\vec{q}\sigma}W(\vec{k}'-\vec{G}'-\vec{k}+\vec{G})\ . \tag{5}$$

In Eq. (5) M is the ionic mass, N is the number of ions per unit volume of the crystal, $W(q)$ is the local form factor of the pseudopotential, and $a_{\vec{G}}(\vec{k})$ is the expansion coefficient of the electronic pseudo wave function at $\vec{k}$ in terms of plane waves (OPW's).

Equation (2) gives the bare (unrenormalized) lifetime. Similar to the case of the effective mass, the lifetime is renormalized[10] due to the many-body effect of the electron-phonon interaction:

$$\tau_t^{-1}(\vec{k},T)=\tau_b^{-1}(\vec{k},T)/(1+\lambda_{\vec{k}})\ , \tag{6}$$

where $\lambda_{\vec{k}}$ is the anisotropic strength of the electron-phonon interaction given by

$$\lambda_{\vec{k}}=2\int_0^\infty d\omega\,\alpha^2F(\vec{k},\omega)/\omega\ .$$

Note that one should realistically use the temperature dependent $\lambda_{\vec{k}}(T)$ in Eq. (6). However, for the low temperatures for which we are mostly concerned in this work, the temperature dependence of $\lambda_{\vec{k}}(T)$ is small.[10]

Experiments such as Azbel'-Kaner cyclotron resonance and surface Landau-level resonance involve a spectrum of electron states ω above the Fermi level. These experiments generally measure an energy-averaged inverse lifetime which is larger than the value at the Fermi level by a factor R:

$$\langle\tau^{-1}(\vec{k},\omega,T)\rangle=R\tau^{-1}(\vec{k},T)\ . \tag{7}$$

For the SLLR experiment,[11] $R=\frac{12}{7}$ and for the AKCR experiment,[12] $R=1.21$.

Generally at low temperatures $\tau^{-1}(\vec{k},T)\propto T^n$ where n runs from 1 to 5. Different power laws arise from differences in the geometry of the effective region of scattering on the Fermi surface.[13] For a large spherical Fermi surface for which the phonon wave vector $\vec{q}$ satisfies $|\vec{q}|\ll k_F$ and for which only normal scattering contributes, a T^3 law can be expected. For the opposite extreme for which $|\vec{q}|\gg k_F$, a linear dependence of T is expected. On the other hand, if the Fermi surface is cylindrical of radial dimension k_r and linear dimension k_l and $k_r\ll|\vec{q}|\ll k_l$, a quadratic dependence can be obtained. Additional processes involving transverse phonons may sometimes give an effective T^5 behavior. A T^3 dependence has been observed in In (Refs. 1-3) and in Al (Ref. 12). T^2 behavior has been seen in Bi (Ref. 14) and in Sb (Ref. 15) and a T^5 dependence in Cd (Ref. 16).

For polyvalent metals such as indium, the character of the wave function changes dramatically near the Bragg planes. Several OPW components of the wave function have appreciable contributions in these regions of the Fermi surface. However, in free-electron-like regions which are far away from the Bragg planes, the dominant contribution comes from only one component. In these regions a 1-OPW model can fairly well describe the nature of the contribution to scattering and hence the temperature dependence of $\tau^{-1}(\vec{k},T)$. Analytical results can be achieved in this case which will give some idea of what to expect for the true temperature dependence for the realistic situation. Such a simple model[3,11] is briefly reviewed below.

A. 1-OPW model (for normal-scattering processes only)

At low temperature, $\vec{q}$ is generally small, and scattering between $\vec{k}$ and $\vec{k}'$ takes place only in the neighborhood of $\vec{k}$. In a free-electron region, $a_G=1$ for $G=0$ and the other a's vanish. Also $v_b(\vec{k})=v_b(\vec{k}')=v$, and we consider the Fermi surface near $\vec{k}$ to be the plane tangent to the true Fermi surface at $\vec{k}$. To terms linear in $|\vec{q}|$, Eq. (5) becomes

$$q_{\vec{k}\vec{k}'\sigma} = -i(2MN\omega_{\vec{q}\sigma})^{-1/2}\hat{e}_{\vec{q}\sigma}\cdot\vec{q}\,W_0 ,$$

where

$$W_0 = \langle \vec{k} \mid W \mid \vec{k} \rangle .$$

The area element on the Fermi surface is $dS' = q\,dq\,d\theta$ where we have used a cylindrical coordinate system centered at $\vec{k}$, and $\vec{q} = \vec{k}' - \vec{k}$ lies on the Fermi-surface plane. We further assume an isotropic phonon spectrum, and use the fact that $\hat{e}_{\vec{q}\sigma}\cdot\vec{q} = q$ for the longitudinal mode and vanishes for the transverse modes. Equation (3) then becomes

$$[\alpha^2 F(\vec{k},\omega)]^{(1)}_{NL} = \frac{W_0^2\omega^2}{8\pi^2\rho v s_L^4} . \tag{8}$$

In the above equation ρ is the ionic mass density MN and $s_L = \omega_{\vec{q}L}/q$ is the speed of sound for the longitudinal mode. Finally Eq. (2) becomes

$$[\tau_b^{-1}(\vec{k},T)]^{(1)}_{NL} = \frac{W_0^2(k_BT)^3}{2\pi\rho v s_L^4}\int_0^\infty \frac{x^2}{\sinh(x)}dx = \frac{7\zeta(3)k_B^3W_0^2}{4\pi\rho v s_L^4}T^3 , \tag{9}$$

where $\zeta(3)$ is the Riemann ζ function with $\zeta(3) = 1.202$. In Eqs. (8) and (9), the subscript NL refers to the longitudinal component of the normal-scattering processes and the superscript represents the 1-OPW wave function.

We can obtain some understanding as to why there is a large anisotropy in the scattering rate by considering the 2-OPW model of Ref. 11. [We find that in Eq. (2.41b) of Ref. 11 the $-(1/2)S$ in the second term should be replaced by $+S$.] The contribution to normal scattering from transverse phonons also has a T^3 dependence, and s_T^4, the transverse speed of sound, occurs in the denominator. The contribution of longitudinal phonons to normal scattering does not change greatly on going from free-electron-like regions on the Fermi surface to regions near Bragg planes (e.g., the ridges of the second-zone surface for In). On the other hand, the contribution from transverse phonons is negligible on free-electron regions where only one OPW is important, but on the ridges the electronic contribution in the transverse-phonon part of the scattering is comparable to the electronic contribution in the longitudinal part. Combining this with the factor $(s_L/s_T)^4 \simeq 50$ for In results in an estimated anisotropy ratio of greater than 10 to 1 for the normal-scattering rate on the ridges compared to that on the free-electron regions.

B. 1-OPW model (for umklapp-scattering processes only)

Umklapp-scattering processes, unlike normal-scattering processes, require, except for $\vec{k}$ on a Bragg plane, a minimum wave vector q_0. Consequently, below a certain temperature $T_u = q_0 s_\sigma/k_B$, umklapp-scattering processes will be frozen out. The present analysis applies best to $\vec{k}$ in the [001], [111], or [100] direction for indium.

As shown by Wagner and Bowers for a 1-OPW model,[11] deviation from the T^3 dependence occurs for the umklapp contribution to $\tau_b^{-1}(\vec{k},T)$. For the longitudinal component, $\tau_b^{-1}(\vec{k},T)$ varies with temperature roughly as

$$[\tau_b^{-1}(\vec{k},T)]^{(1)}_{UL} \propto T\exp(-q_0 s_L/k_BT) , \tag{10}$$

and the transverse component varies as

$$[\tau_b^{-1}(\vec{k},T)]^{(1)}_{UT} \propto T^2\exp(-q_0 s_T/k_BT) . \tag{11}$$

In Eqs. (10) and (11), the subscripts UL and UT refer to the longitudinal and transverse components of the umklapp-scattering processes, respectively. The superscript 1 denotes the 1-OPW wave function. The slow transverse sound speed s_T (as compared to the longitudinal speed s_L) might also have a prominent effect on the anisotropy of the scattering rate. Since $(\vec{q}+\vec{G})\cdot\hat{e}_{\vec{q}T} = 0$ in the matrix element in Eq. (5) for the [001], [111], and [100] directions for indium, the transverse components to $\tau_b^{-1}(\vec{k},T)$ for these directions are negligibly small. However, coupling to the transverse modes increases sharply away from these free-electron-like regions, especially near the ridges. Consequnetly a large umklapp transverse contribution might result near the ridges. Similar results have been obtained in a realistic calculation in aluminum.[17] As we shall see in the following sections, our present calculations in indium are also consistent with this observation both with respect to the non-T^3 behavior and large umklapp-scattering rate near the ridges.

III. METHOD OF CACULATION

The frequency integral in Eq. (2) for the inverse lifetime $\tau_b^{-1}(\vec{k},T)$ for a given $\vec{k}$ direction is done numerically using values of $\alpha^2F(\vec{k},\omega)$ calculated for the corresponding $\vec{k}$ direction. The pseudopotential model of Ashcroft and Lawrence[18] (AL) is used to generate the Fermi-surface points $\vec{k}$, band velocity $v_b(\vec{k})$, and the electronic wave function in terms of up to a maximum of seven OPW's. Fermi surface data $\vec{k}, \vec{v}_b(\vec{k})$, $a_{\vec{G}}(\vec{k})$, and dS in the irreducible section of the Brillouin zone are calculated in the extended-zone scheme on a grid system of $\cos\theta$ and ϕ, where θ is the polar angle measured from [001] and ϕ is the azimuthal angle measured from [100] on the basal plane. A realistic-phonon model[19] is used to obtain the phonon frequencies $\omega_{\vec{q}\sigma}$ and polarization vectors $\hat{e}_{\vec{q}\sigma}$. The anisotropic function $\alpha^2F(\vec{k},\omega)$ for both one and many-OPW wave functions are calculated for several $\vec{k}$ directions on both the second- and third-zone surfaces using a Monte Carlo method and the AL pseudopotential for the electron-phonon matrix element. In this calculation we determine $\vec{k}'$ values at random on the Fermi surface in the extended-zone scheme. From the information of $\vec{k}$ and $\vec{k}'$, $\vec{q}$ and $\vec{G}$ are determined from Eq. (4), and the corresponding phonon frequency $\omega_{\vec{q}\sigma}$ and polarization vector $\hat{e}_{\vec{q}\sigma}$ are obtained using the phonon model.[19] The electron-phonon matrix elements $g_{\vec{k}\vec{k}'\sigma}$ are then calculated and the surface integral in Eq. (3) is obtained by summing over all $\vec{k}'$ and polarizations σ. The δ function

in Eq. (3) is taken care of by dividing the frequency range into equally spaced intervals or bins. The detailed method of calculation has been reported earlier.[9,20] The frequency integral in Eq. (2) is performed for $\alpha^2F(\vec{k},\omega)$ for both 1- and many-OPW wave functions simultaneously for temperatures from 0.1 to 10 K.

At very low energy, $\alpha^2F(\vec{k},\omega)$ is proportional to ω^2. Thus at very low temperatures the inverse lifetime is given by an integral of the function $f(x)=x^2/\sinh(x)$ [see Eq. (2)] where $x=\omega/k_BT$. This function has a low-energy peak so that at low temperatures most of the contribution to $\tau_b^{-1}(\vec{k},T)$ comes from the low-energy part of $\alpha^2F(\vec{k},\omega)$.

The method of calculation of $\alpha^2F(\vec{k},\omega)$ we used[9,20] for the mass enhancement $\lambda_{\vec{k}}$ produces a uniform error in $\alpha^2F(\vec{k},\omega)$ at all ω values. This is quite satisfactory in calculating $\lambda_{\vec{k}}$ since for this quantity there is only a slight $(1/\omega)$ weighting toward low frequencies. With a uniform error in $\alpha^2F(\vec{k},\omega)$ the percentage error at low frequencies where $\alpha^2F(\vec{k},\alpha)$ is small becomes quite large, and it is only at low frequencies that α^2F is needed for the low temperature τ^{-1}.

For most of the $\vec{k}$ directions for which $\alpha^2F(\vec{k},\omega)$ has already been calculated,[9,20] we incorporate the following modifications for low energy. The first five frequency bins corresponding to the lowest 5% of the total phonon range are divided into 20 equally spaced bins, and, depending on the location of $\vec{k}$ on the Fermi surface, 100 to 1000 extra random $\vec{k}'$ vectors on each Fermi-surface grid square are generated in the neighboring region of $\vec{k}$ (a larger number of random vectors are generated for $\vec{k}$ on the ridges). For the rest of the Fermi surface 20 extra $\vec{k}'$ vectors are generated on each grid square. Then the integration in Eq. (2) is carried out in three steps. In the first step, only the normal-scattering contribution to $\alpha^2F(\vec{k},\omega)$ for the first 20 bins is considered, i.e., for the lowest 5% of the phonon frequencies. Because $\alpha^2F(\vec{k},\omega)$ is proportional to ω^2 in this low-frequency region, the integral is solved numerically using

$$\alpha^2F(\vec{k},\omega)=C\omega^2 \tag{12}$$

for the lowest values of ω where C is obtained by integrating both sides of Eq. (12) over the low-ω range. Umklapp-scattering contributions to $\tau_b^{-1}(\vec{k},T)$ for this same low-energy range are then evaluated by a frequency sum of the form

$$\sum_{i=1}^{N}\alpha^2F(\vec{k},\omega_i)[\ln\tanh(\omega/k_BT)]\Big|_{\omega_{i-1}}^{\omega_i} \tag{13}$$

using $N=20$. α^2F for Eq. (13) is calculated considering only umklapp scattering. In the third step, the total (including both normal and umklapp scattering) $\alpha^2F(\vec{k},\omega)$ for larger ω is used for the rest of the integral using a sum as in Eq. (13).

Results obtained in all three steps are added to give the value of $\tau_b^{-1}(\vec{k},T)$. The renormalized value $\tau_t^{-1}(\vec{k},T)$ is then calculated from Eq. (6) using the corresponding value of $\lambda_{\vec{k}}$ at $\vec{k}$.[9,20]

IV. ANISOTROPY OF THE LIFETIME ON THE SECOND-ZONE SURFACE

We discuss the anisotropy and temperature dependence of the inverse lifetime in terms of the T^3 coefficient of Eq. (1). For the bare lifetime we have $\gamma_b(\vec{k})$ while for the renormalized or true value we have $\gamma_t(\vec{k})$ related to γ_b through $\lambda_{\vec{k}}$ as in Eq. (6).

The calculated values of $\gamma_b(\vec{k})$ obtained from Eq. (2) for a few $\vec{k}$ directions along the center of the free-electron-like hexagonal and square faces and on the ridges of the second-zone surface are listed in Table I. Both the normal- and total-scattering contribution for the many-OPW case and also the normal-scattering contribution for the 1-OPW case for temperatures from 1.5 to 4.2 K are listed. These are compared to the values calculated from the simple 1-OPW model given by Eq. (9). In using Eq. (9) we need the velocity of sound s_L which enters to the fourth power. There is a rather large anisotropy in the velocity so the γ from Eq. (9) is quite sensitive to the mean value of s_L we use. On the other hand, the value shown in the next to last column of Table I is obtained by doing a sum over the true Fermi surface using the actual anisotropic velocities. This accounts for the differences

TABLE I. Local value of the T^3 coefficient of the bare lifetime $\gamma_b(\vec{k})$ (10^7 s^{-1}K^{-3}) for a few $\vec{k}$ directions on the second-zone surface.

	Present calculation using Eq. (2) for temperatures 1.5–4.2 K			Calculation from Eq. (9) for 1-OPW model
	Many OPW		1 OPW	
Direction $\vec{k}$	Total	Normal	Normal	Normal
[001] point 11[a]	1.31–2.81	1.31–1.74	1.83–2.20	1.90
[111] point 4	2.08–2.96	2.08–2.44	2.12–2.26	1.80
[100]	1.76–10.90	1.70–2.56	2.06–2.25	2.10
[110] point 1	55.64–62.48	14.06–13.36	1.53–1.64	4.13
Point 8 on the ridge	43.15–73.16	23.36–34.65	1.43–1.55	2.76

[a]The point numbers refer to the inset in Fig. 1.

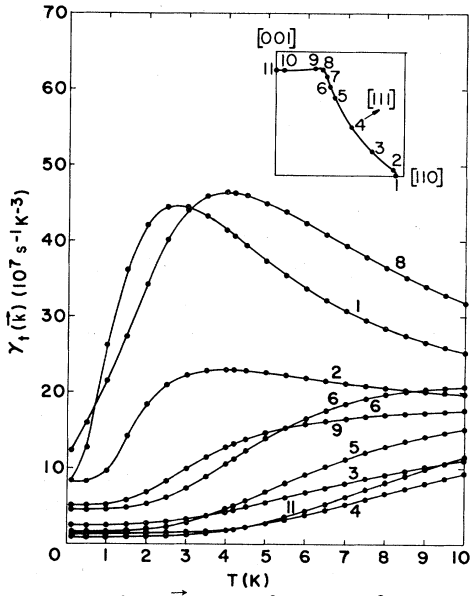

FIG. 1. Plots of $\gamma_t(\vec{k})$ as a function of temperature for points along the [110] orbit on the second-zone surface. The location of the points on the orbit is shown in the inset.

between the two columns, for example, in the [111] direction which is a free-electron-like region. As can be seen from this table, 1-OPW results both from the simple and realistic model calculations agree very well with the realistic many-OPW calculations for the free-electron-like regions, ([001], [111], and [100] directions) not only for the normal-scattering part but even for the total contribution. However, on the ridges which are close to Bragg planes, mixing of many-OPW components are quite appreciable. Consequently 1-OPW results for these directions fail to reflect the true value of the lifetime. These observations are consistent with the analysis of Sec. II. Hereafter we consider only the many-OPW results for $\gamma(\vec{k})$.

The calculated values of $\gamma_t(\vec{k})$ as a function of temperature for several points along the [110] and [011] orbits on the second-zone surface (in the reduced-zone scheme) for temperatures from 0.1 to 10 K are plotted in Figs. 1 and 2. Location of these points are shown in the inset of these figures. At the lowest temperatures a T^3 behavior in the free-electron-like regions (points 11 and 3–5 in Fig. 1 and points 1 and 5–7 in Fig. 2) is quite apparent from these plots. With the onset of umklapp scattering at higher T, the T^3 law does not hold and the inverse lifetime is found to be enhanced. We also see a huge anisotropy (in excess of 30:1 at 3 K) at low temperatures as we go from the free-electron-like regions to the ridges. This is attributable in part to the large umklapp contribution at the ridges (points 1, 2, and 7–9 in Fig. 1 and point 3 in Fig. 2). To show this effect we also plot the contribution to $\gamma_t(\vec{k})$ from normal-scattering processes as a function of temperature in Figs. 3 and 4. Two characteristic features can immediately be observed when we compare the values of Figs. 1 and 2 with the corresponding values of Figs. 3 and 4, respectively. (a) The normal part of the inverse lifetime shows a T^3 dependence even at relatively high temperature, and (b) the umklapp threshold temperature T_U decreases in going from free-electron-like regions to the ridges.

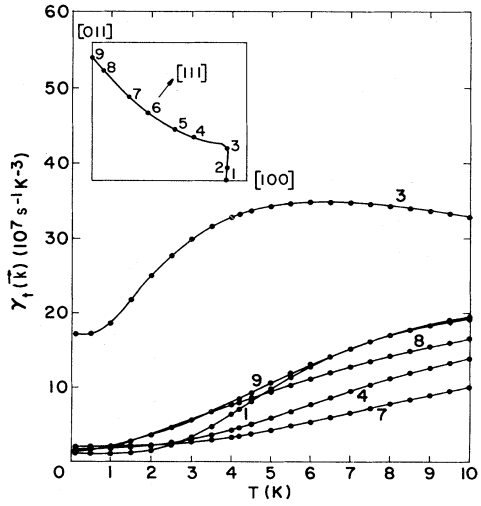

FIG. 2. Plots of $\gamma_t(\vec{k})$ as a function of temperature for points along the [011] orbit on the second-zone surface. The location of the points on the orbit is shown in the inset.

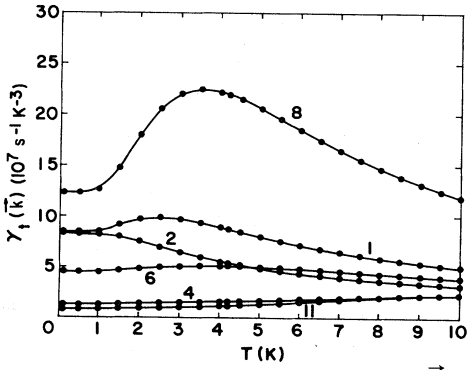

FIG. 3. Plots of the normal contribution of $\gamma_t(\vec{k})$ as a function of temperature for some of the points shown in Fig. 1 along the [110] orbit on the second-zone surface.

Calculated $\gamma_t(\vec{k})$ as a function of $\vec{k}$ for the [110] and [011] orbits are shown in Figs. 5 and 6 corresponding to the values plotted in Figs. 1 and 2. It can be seen from these plots that $\gamma_t(\vec{k})$ is sharply peaked on the ridges. These peaks get broader with an increase in temperature

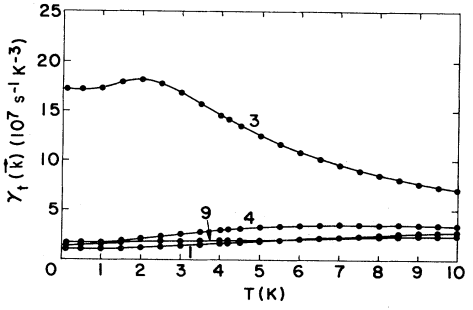

FIG. 4. Plots of the normal contribution of $\gamma_t(\vec{k})$ as a function of temperature for some of the points shown in Fig. 2 along the [011] orbit on the second-zone surface.

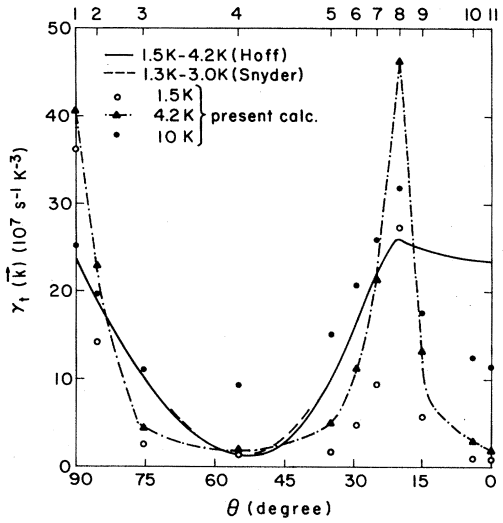

FIG. 5. Plots of the calculated $\gamma_t(\vec{k})$ as a function of angle θ measured from [001] along the [110] orbit on the second-zone surface for several values at temperature (θ increases from right to left). Calculated values at 4.2 K are shown by the dashed-dotted curve. This is compared to the corresponding values of Hoff *et al.* (Refs. 1 and 3) (shown by the solid curve) obtained from their inversion scheme. Also plotted are the measured values of Snyder (Ref. 5) (shown by the dashed curve) for a limited region around [111]. See also Fig. 1 for the location of the points identified by the numbers along the horizontal axis.

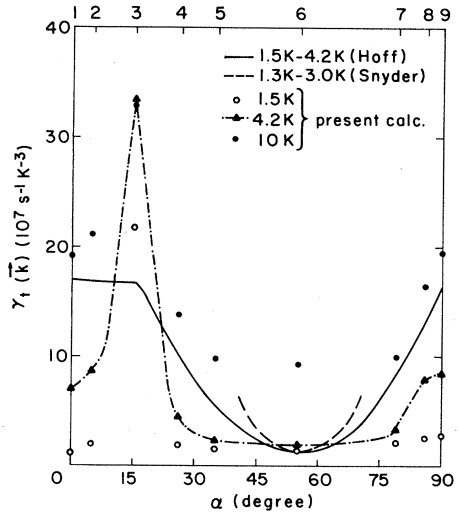

FIG. 6. Plots of the calculated $\gamma_t(\vec{k})$ as a function of angle α measured from [100] along the [011] orbit on the second-zone surface for several values of temperature. Calculated values at 4.2 K are shown by the dashed-dotted curve. This is compared to the corresponding values of Hoff *et al.* (Refs. 1 and 3) (shown by the solid curve) obtained from their inversion scheme. Also plotted are the measured values of Snyder (Ref. 5) (shown by the dashed curve) for a limited region around [111]. See also Fig. 2 for the location of the points identified by the numbers along the horizontal axis.

and the large anisotropy washes out noticeably above 9 or 10 K.

Also plotted in Figs. 5 and 6 are the values of $\gamma_t(\vec{k})$ reported by Hoff *et al.*[1,3] (the solid curve) and the experimental results of Snyder[5] (the dashed curves) in the neighborhood of the [111] direction. The results of Hoff *et al.* for individual $\vec{k}$ points were obtained by them by an inversion scheme from their experimental RFSE measurements on extremal cyclotron orbits. That is, they obtained orbit-averaged $\overline{\gamma}_t$ for each orbit directly from their experiment. For orbit j, $\overline{\gamma}_{tj}$ is related to the point values of $\gamma_t(\vec{k})$ on the orbit by

TABLE II. Comparison of the calculated values of $\gamma_t(\vec{k})$ with experiment for a few $\vec{k}$ directions on the second-zone surface. See Fig. 1 for the location of the $\vec{k}$ directions.

Direction	Method	$\gamma_t(\vec{k})\times 10^7$ s^{-1}K^{-3}	Range of temperature	Reference
[111]	Theory	1.34—1.91	1.5—4.2 K	Present calculation
	Limiting-point RFSE	1.21±0.33[a]	1.3—3.0 K	5
	Limiting-point RFSE	1.20±0.08	1.5—4.2 K	3
9° from [111]	Theory	2.54—4.42	1.5—4.2 K	Present calculation
	Limiting-point RFSE	3.37±0.06[b]	1.3—4.0 K	6
Point 8 in Fig. 1	Theory	27.31—46.30	1.5—4.2 K	Present calculation
	SLLR	7.6[c]		7

[a]This value is obtained by multiplying the reported value of the T^3 coefficient of the inverse mean-free parth by the factor $v_b/(1+\lambda_k)=1.7\times10^8$ cm s^{-1}/1.55$=1.1\times10^8$ cm s^{-1}.

[b]This value is obtained by reading the value of the T^3 coefficient of the inverse mean-free path from Fig. 5 of Krylov and Gantmakher (Ref. 6) and then by multiplying this value by the factor 1.1×10^8 cm s^{-1}, as in a above.

[c]This value is obtained by multiplying the reported value by the factor $1/R=\frac{7}{12}$ of Eq. (7).

$$\bar{\gamma}_{tj}=\int_j \gamma_t(\vec{k})dt \Big/ \int_j dt=\left[\int_j \gamma_t(\vec{k})dk \Big/ v_{b\perp}(\vec{k})\right] \Big/ \left[\int_j dk \Big/ v_{b\perp}(\vec{k})\right], \tag{14}$$

where $v_{b\perp}(\vec{k})$ is the component of $v_b(\vec{k})$ perpendicular to $\vec{H}$ and the integration is over the jth orbit.

Hoff *et al.*[1,3] then attempted to extract the point values of γ on the orbits from the orbit-averaged $\bar{\gamma}$ by measuring many intersecting orbits and assuming that $\gamma(\vec{k})$ can be accurately represented by a few terms in a properly symmetrized Fourier expansion. The point values were than obtained by inverting the expansion.

Hoff *et al.*[1,3] have performed the RFSE experiments for 18 central orbits on the second-zone surface for temperatures from 1.5 to 4.2 K. A T^3 dependence of the orbit-averaged inverse lifetime $\bar{\tau}^{-1}(T)$ was observed for each of these orbits. They have also performed the inversion scheme using the Fermi-surface data of Ashcroft and Lawrence[18] in which they used a constant value of $\lambda=0.6$ over the entire second-zone surface. They have shown that the hole-surface data can be fit by a least-squares method to a precision of about 7% to a five-term Fourier expansion.

Looking again at our results in Figs. 5 and 6, we see they produce a minimum in $\gamma_t(\vec{k})$ for the [111] direction (point 4 in Fig. 5 and point 6 in Fig. 6) with a value which agrees with both the inversion result and the experiments of Snyder.[5] We disagree along the [001] direction (point 11 in Fig. 5) where we get close to an absolute minimum while the inversion scheme gives a large value. We also disagree in the [100] direction (point 1 or $\alpha=0$ in Fig. 6). Although $\gamma_t(\vec{k})$ obtained from the inversion scheme is quite large near the ridges, its variation is rather slow in this region compared to the sharp peaks shown by our calculated values. This lack of sharpness in the inversion values could be a result of the choice of low-order, smoothly varying basis functions. Since the anisotropy near the ridges for our calculated results is confined to a very small distance in k space, a large number of terms in the Fourier expansion would be necessary to describe the true anisotropy. Higher-order expansions, however, give spurious oscillations in $\gamma_t(\vec{k})$ and have little practical use. Furthermore, the inversion scheme is not unique using a finite number of terms because an infinite number of functions is generally required.

We can compare our results with other local measurements (see Table II). The limiting-point RFSE results of Snyder[5] show that the variation of the local value near [111] follows a parabolic law of the form

$$\gamma_t(\vec{k})=(1.21\pm0.33)\times10^7 + (0.023\pm0.003)\times10^7\chi^2\ \mathrm{s^{-1}K^{-3}} \tag{15}$$

for $|\chi|<15°$, where χ is the angle in degrees measured from [111]. This is also plotted in Figs. 5 and 6. Hoff[3] has obtained a value $(1.21\pm0.08)\times10^7\ \mathrm{s^{-1}K^{-3}}$ for the [111] limiting point. Our calculated value (with no adjustable parameters) of $(1.34\text{—}1.91)\times10^7\ \mathrm{s^{-1}K^{-3}}$ between 1.5—4.2 K for this direction is in very good agreement with the above measurements. However, our results do not increase as rapidly as Eq. (15) on moving away from [111]. On the other hand, good agreement is obtained for points making an angle of 9° from [111] between the RFSE result of Krylov and Gantmakher[6] and our calculated values for a similar range of temperatures (see Table II). Only one value of $\gamma_t(\vec{k})$ is available to date near the ridges. Doezma and Koch[7] found a value $7.6\times10^7\ \mathrm{s^{-1}K^{-3}}$ for the point 8 on the ridge (see Fig. 1). The calculated value at this point is much larger (4—6 times) than the measured value. However, the identification of the resonant electrons in the SLLR experiment is only tentative and it is possible that the SLLR value is in fact located elsewhere on the Fermi surface.[1]

Because of the uncertainties of the results from the inversion scheme, it is more meaningful to make a direct comparison between theory and experiment for the calculated renormalized orbit-averaged T^3 coefficient $\bar{\gamma}_t$ given by the orbit average of $\gamma_t(\vec{k})$. The line integral is carried out along different orbits using the calculated local values of $\gamma_t(\vec{k})$. In Fig. 7 we plot $\bar{\gamma}_t$ as a function of temperature for a few central orbits on the second-zone surface over the range of 1.5 to 10 K. We definitely see deviations from a purely cubic temperature dependence of the orbit-averaged inverse lifetime. Our results below 3 K are not very accurate (which is discussed in Sec. VI), and for the range of 3 to 10 K deviations from T^3 are relatively small for some of these orbits.

A comparison is made in Table III between the present calculation and the RFSE results of Hoff *et al.*[1,3] for 18 central orbits on the second-zone surface. These values are also plotted in Fig. 8. Our results listed in Table III are for the experimental range of temperature of 1.5 to 4.2 K, while our results plotted in Fig. 8 are for several temperatures between 1.5 and 10 K. The calculated values

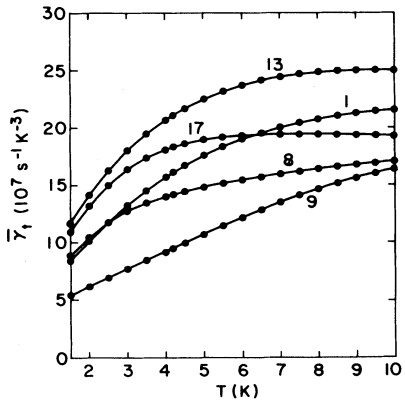

FIG. 7. Plots of the orbit-averaged values $\bar{\gamma}_t$ as a function of temperature for a few orbits on the second-zone surface. Numbers identify the orbits which are listed in Table III. Note that orbits Nos. 8 and 9 are the [110] and [011] central orbits, respectively.

TABLE III. Comparison of the calculated orbit-averaged T^3 coefficient of lifetime with the experimental results of Hoff (Ref. 3). All orbits are central and on the second-zone surface. θ refers to the polar angle measured from [001] and ϕ is the azimuthal angle measured from [100] on the basal plane. λ_{orb} is the orbit-averaged mass enhancement.

Orbit No.	θ (degrees)	ϕ (degrees)	λ_{orb}	$\bar{\gamma}_t \times 10^7$ s^{-1}K^{-3} Present calculation $1.5 \leq T \leq 4.2$ K	Experiment $1.5 \leq T \leq 4.2$ K
1	90	10	0.62	8.44—16.24	16.5±1.7
2	90	13	0.60	8.79—15.63	16.5±0.8
3	90	15	0.60	9.12—16.16	16.16±1.8
4	90	18	0.57	9.11—16.78	16.9±0.8
5	90	23	0.58	9.12—16.70	17.7±0.9
6	90	30	0.56	7.06—13.56	14.3±1.4
7	90	37.5	0.55	6.54—12.22	14.0±1.0
8[a]	90	45	0.55	8.73—14.18	15.1±0.7
9[b]	42.7	0	0.59	5.34— 9.48	9.9±0.5
10	42.9	5.9	0.59	5.04— 9.18	10.0±0.5
11	43.1	11.6	0.59	4.32— 8.53	10.4±0.5
12	43.6	17.6	0.59	4.77— 9.61	10.7±0.5
13	10	0	0.60	11.67—21.10	18.5±1.9
14	75	0	0.59	7.49—15.15	14.9±1.5
15	78	0	0.59	6.22—13.48	15.2±0.7
16	82.5	45	0.55	8.74±14.89	15.1±0.8
17	75	45	0.57	10.88—18.32	16.5±1.0
18	47.8	14	0.59	4.57— 9.01	12.1±1.2

[a]This is the [110] central orbit.
[b]This is the [011] central orbit.

agree reasonably well with experiment in the high-temperature part of this range (3 to 4.2 K), but below 3 K only qualitative agreement exists. A fairly large anisotropy in the local value of $\gamma_t(\vec{k})$ is washed out by averaging over the orbits leaving an anisotropy of only 2:1 in $\bar{\gamma}_t$.

Thus we see that there is reasonable agreement between our calculated results at 4.2 K (our best low-temperature results since the errors in the calculation increase at lower temperatures) and the experimental results[1,3] for the orbit-averaged $\bar{\gamma}_t$. However, there is not such good agreement between our calculated local $\gamma_t(\vec{k})$ (which we used in obtaining $\bar{\gamma}_t$) and those extracted from the experimental $\bar{\gamma}_t$ by the inversion scheme. We believe this shows that the local results in Refs. 1—3 obtained by the inversion scheme are of limited accuracy.

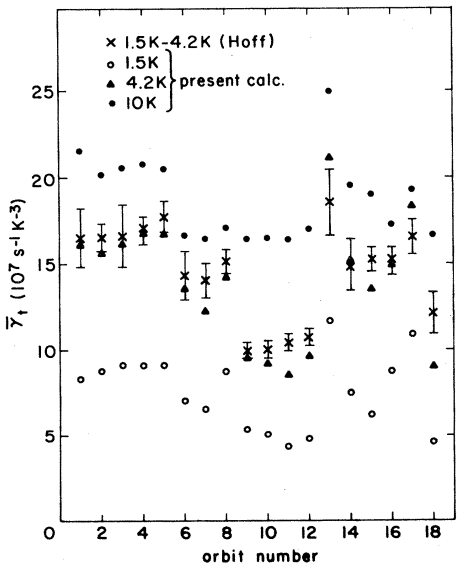

FIG. 8. Comparison of the calculated orbit-averaged values with the results of Hoff *et al.* (Refs. 1 and 3) for 18 central orbits on the second-zone surface. See also Table III. Calculated values are shown for several temperatures.

V. ANISOTROPY OF THE LIFETIME ON THE THIRD-ZONE SURFACE

Our calculated $\gamma_t(\vec{k})$ for seven points on the central [110] belly orbit (β') on the β arm surface is shown in Fig. 9 for temperatures from 1.5 to 10 K. A large value is obtained for point A mainly due to the umklapp-scattering processes. The values of $\gamma_t(\vec{k})$ at A and A' should be identical since they are the same point in the reduced-zone scheme. However, the calculations are carried out in the extended-zone scheme for which A and A' are separate points. The extent to which the two curves differ in Fig. 9 gives an indication of the error in our calculations. We also find a large anisotropy (8:1 at 3 K) in $\gamma_t(\vec{k})$ on the third-zone surface.

Hoff and co-workers[2,3] have performed RFSE measurements of the orbit-averaged $\bar{\gamma}_t$ for 13 central belly orbits on the third-zone β-arm surface. They have tried to obtain the local value using an inversion scheme similar to that described in the previous section. A single term has been found sufficient to adjust all the experimental data within the experimental error (they have obtained a constant value $\bar{\gamma}_t = 23 \times 10^7$ s^{-1}K^{-3}). However, since these 13 orbits do not represent a fine network of orbits on the entire third-zone surface, they have concluded that the in-

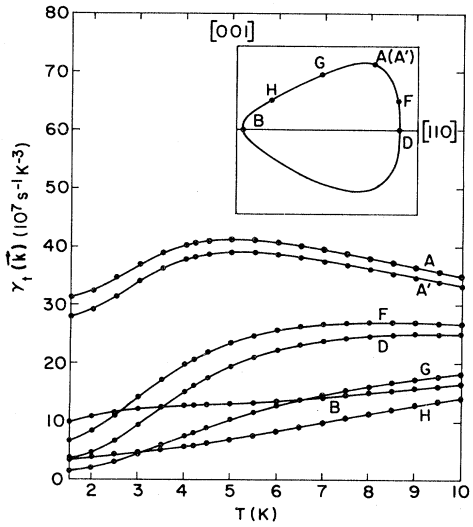

FIG. 9. Plots of $\gamma_t(\vec{k})$ as a function of temperature for points along the central [110] belly orbit on the third-zone surface. The location of the points are shown in the inset.

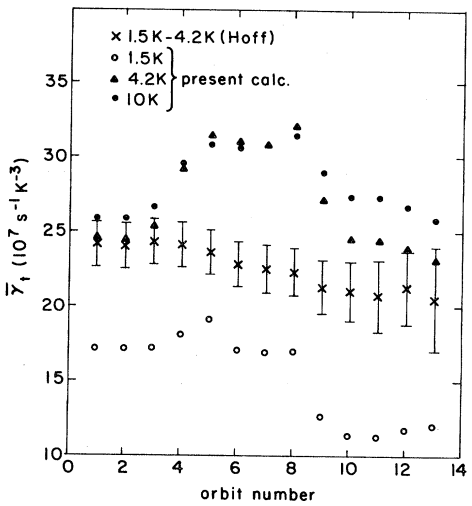

FIG. 11. Comparison of the calculated orbit-average values with the results of Hoff for 13 central orbits on the third-zone surface. See also Table IV. Calculated values are shown for several temperatures. Note that the ordinate does not begin at zero.

version scheme is not applicable to the data obtained from the measurements on these orbits.

The calculated values of the orbit-averaged $\bar{\gamma}_t$ as a function of temperature for a few orbits are shown in Fig. 10. As in the case of the second-zone surface, deviation from a T^3 dependence is found below 5 K. We also compare our results of $\bar{\gamma}_T$ with Hoff's RFSE measurements for 13 central orbits in Fig. 11. These values are summarized in Table IV, which also lists the value of $\bar{\gamma}_t$ for the first orbit (this is the [110] belly orbit β') obtained by Castaing and Goy[4] from the AKCR experiment. The calculated values of $\bar{\gamma}_t$ in the temperature range of 3 to 10 K agree reasonably well with the RFSE results at least for the first 3 and the last 4 orbits. Below 3 K only qualitative agreement is obtained for all these orbits.

A puzzling difference between the AKCR and RFSE result for the [110] orbit is that the AKCR value is about half as large as the RFSE value. A similar difference is also found between the calculated value and the AKCR result.

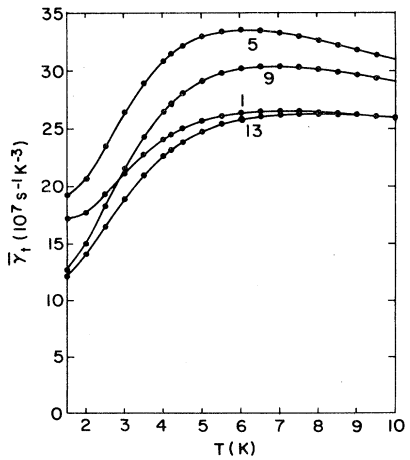

FIG. 10. Plots of the orbit-averaged values $\bar{\gamma}_t$ as a function of temperature for a few orbits on the third-zone surface. Numbers identify the orbits which are listed in Table IV. Note that orbit No. 1 is the [110] belly orbit β'.

Hoff *et al.* have also performed measurements of $\bar{\gamma}_t$ for a limiting-point orbit around the point A (see Fig. 9) on the β arm. They have obtained a value of $(19\pm3.5)\times10^7$ s^{-1}K^{-3} for the temperature range from 1.5 to 4.2 K. Since this orbit covers a very small region around A, this value of $\bar{\gamma}_t$ can be assumed to be approximately equal to the local value $\gamma_t(\vec{k})$ at A. However, the calculated value in this temperature range is found to be (31.22 to 40.63)$\times10^7$ s^{-1}K^{-3} (see Fig. 9), which is much larger than the experimental value. A value of $\gamma_t(\vec{k})=(19\pm3.5)\times10^7$ s^{-1}K^{-3} at this point is not consistent with Hoff's orbit-averaged value of $\bar{\gamma}_t=(24.1\pm1.5)\times10^7$ s^{-1}K^{-3} for the [110] orbit unless $\gamma_t(\vec{k})$ at other points on this orbit is equal to or larger than the value at A. From our realistic calculations, we find that a large maximum occurs at point A (see Fig. 9). A large maximum at point A is not consistent with both the limiting-point measurement and the orbit-averaged value of Hoff *et al.*

There is an explanation for some of the differences between the calculated values and results obtained from the RFSE experiment. Hoff *et al.*[2,3] have used the model Fermi surface of Harmans[21] and a constant value of $\lambda=0.8$ to obtain the orbit time t. We have used the pseudopotential model of Ashcroft and Lawerence[18] for the Fermi surface and realistic anisotropic values of $\lambda_{\vec{k}}$ along the orbits. However, we believe this use of different models for the analysis can not explain all of the differences between our results on the third-zone surface.

VI. CONCLUSIONS

Overall, fairly good agreement is achieved between the calculated values of the orbit-average T^3 coefficient $\bar{\gamma}_t$ of

TABLE IV. Comparison of the calculated orbit-averaged T^3 coefficient of lifetime with the experimental results of Hoff (Ref. 3). Also listed is the orbit-averaged value of Castaing and Goy (Ref. 4), as CG in the table below) for the [110] orbit, which is orbit No. 1 in this table. All orbits are central and on the third-zone surface. θ refers to the polar angles measured from [001] and ϕ is the azimuthal angle measured from [100] on the basal plane. λ_{orb} is the orbit-averaged mass enhancement.

				$\bar{\gamma}_t \times 10^7$ s^{-1}K^{-3}		
					Experiment	
	θ	ϕ		Present calculation	$1.5 \leq T \leq 4.2$ K	
Orbit	(degrees)	(degrees)	λ_{orb}	$1.5 \leq T \leq 4.2$ K	Hoff	CG
1	90	45	0.75	17.17—24.45	24.1±1.5	10[a]
2	90	40	0.75	17.14—24.43	24.0±1.5	
3	90	35	0.75	17.21—25.37	24.3±1.5	
4	90	30	0.75	18.09—29.17	24.1±1.5	
5	90	25	0.76	19.10—31.39	23.6±1.5	
6	90	20	0.76	17.07—30.85	22.8±1.5	
7	90	15	0.76	16.92—30.77	22.5±1.6	
8	90	10	0.76	16.99—32.06	22.3±1.6	
9	90	0	0.75	12.67—27.12	21.3±1.8	
10	90	−7.5	0.74	11.37—24.52	21.0±2.0	
11	90	−10	0.74	11.28—24.44	20.7±2.4	
12	90	−15	0.74	11.77—23.96	21.3±2.5	
13	90	−25	0.74	12.04—23.11	20.5±3.5	

[a]This value is obtained by dividing the reported value of Castaing and Goy (Ref. 4) by the factor $R=1.21$ in Eq. (7).

inverse lifetime with the extensive measurements of Hoff *et al.*[1-3] on the second-zone surface in indium for temperatures of 3 to 4 K. We emphasize that no adjustable parameters were used in the model calculations. Good agreement is also obtained for the calculated local values of $\gamma_t(\vec{k})$ on the second-zone surface with the limiting-point RFSE measurements. However, our local values of $\gamma_t(\vec{k})$ have larger and sharper peaks on the ridges than do the values found by Hoff *et al.*[1-3] from their inversion scheme. We also have a much lower value of $\gamma_t(\vec{k})$ in the [001] direction ($\theta=0$ in Fig. 5) and in the [100] direction ($\alpha=0$ in Fig. 6) than do Hoff *et al.*

Our calculations clear up a problem that was recognized with the inversion results of Hoff *et al.* from the beginning. This was how one could reconcile the large inverse lifetime or scattering rate in the [100] and [001] directions compared to the [111] direction when all three directions are in nearly-free-electron regions? One would expect on the basis of the 2-OPW model that the inverse lifetime would be comparable in all three directions and it would be lower than in other directions. This is what we find with our detailed realistic calculations. Since we also agree reasonably well with orbit-averaged data of Hoff *et al.*, we conclude that the problem is with the inversion used by Hoff *et al.*

There is not as good agreement between our calculations and the measurements of Hoff *et al.* of the orbit-averaged $\bar{\gamma}_t$ on the third-zone surface as on the second-zone surface. However, both the calculated and experimental results are more sensitive on the third-zone surface to the band model used. Hence the third-zone-surface results are probably less accurate than the second-zone-surface results.

The calculated values of $\gamma_t(\vec{k})$ below 3 K are not as accurate as above 3 K. A major difficulty at low temperature is the numerical limitation in calculating the low-energy spectrum of $\alpha^2F(\vec{k},\omega)$ by the Monte Carlo method. Much care has been taken to reduce numerical error by generating up to 1000 extra random vectors at low phonon energy and by reducing the bin width for the energy integration. Comparing local values of $\gamma_t(\vec{k})$ obtained using $\alpha^2F(\vec{k},\omega)$ from calculations with different degrees of accuracy, we find an error of 6% at 1.5 K and less than 4% above 4.2 K for the [110] orbit on the second-zone surface. Another error estimate for the local value is obtained by comparing values of $\gamma_t(\vec{k})$ for the equivalent points A and A' on the third-zone [110] belly orbit (see Figs. 1 and 13). This shows an error of 10% at 1.5 K and less than 5% at 4.2 K. Considering all these facts we feel that our results have errors of 10% or greater below 3 K.

There is another noteworthy difference between theory and experiment. The calculated values of $\gamma_t(\vec{k})$ show T^3 behavior only in the free-electron-like regions. Deviation from purely cubic temperature dependence in $\gamma_t(\vec{k})$ is expected from theory and is found in our calculations for the non—free-electron-like regions. When averaged over the orbits, we still obtain noticeable deviation from T^3 behavior. On the other hand, the experiments show a T^3 behavior for every orbit-averaged value over the entire Fermi surface. This difference can perhaps be resolved if more experiments are performed to obtain the local values, especially on the ridges.

A major problem in comparing with experiment is the difference between different experiments. As noted in Sec. IV, the SLLR value[7] of $\gamma_t(\vec{k})$ along one direction on the second zone is much smaller than the corresponding RFSE values[1,3] (or than our calculated values). In the preceding section we have also seen a large difference for a third-zone orbit where the AKCR value[4] is much smaller than the RFSE values[2,3] (or again than our calculated values). The reason for such a large discrepancy is not understood.

We finally wish to comment on the fact that we have not included a spin-orbit interaction in determining our Fermi surface or our electronic wave functions. Such an interaction is important[22,23] with regard to the detailed shape of the Fermi surface near W and T on the second-zone hole surface (see Ref. 22 for the notation) and at the junction of the β arms of the third-zone electron surface in the [100] direction. Thus we would not expect our calculated lifetimes to be as accurate in those regions as elsewhere. Note, however, that none of the orbits of Hoff *et al.*[1-3] on the second-zone surface is near the W or T points, and that none of their orbits on the third-zone surface is in the region of the junction of the two arms.

ACKNOWLEDGMENTS

This research was supported by the National Science Foundation under Grants Nos. DMR-80-06939 and DMR-81-17013. One of us (J.C.S.) wishes to thank Dr. A.B.M. Hoff, Dr. D. G. de Groot, and Dr. R. Griessen for valuable discussions and for their hospitalitiy.

*Present address: Department of Physics, The University of Texas at Austin, Austin, TX 78712.

[1]A. B. M. Hoff, D. G. de Groot, and D. L. Randles, J. Phys. F **6**, L141 (1976).

[2]A. B. M. Hoff and D. G. de Groot, J. Low. Temp. Phys. **29**, 467 (1977).

[3]A. B. M. Hoff, thesis, Free University, Amsterdam, 1977.

[4]B. Castaing and P. Goy, J. Phys. C **6**, 2040 (1973).

[5]P. M. Snyder, J. Phys. F **1**, 363 (1971).

[6]I. P. Krylov and V. F. Gantmakher, Zh. Eksp. Teor. Fiz. **51**, 740, (1966) [Sov. Phys.—JETP **24**, 492 (1967)].

[7]R. E. Doezma and F. Koch, Phys. Cond. Matter **19**, 17 (1975).

[8]P. G. Tomlinson and J. C. Swihart, Phys. Cond. Matter **19**, 117 (1975).

[9]B. K. Bhattacharyya and J. C. Swihart, J. Phys. F **14**, 1651 (1984).

[10]G. Grimvall, *The Electron-Phonon Interaction in Metals,* in Vol. 16 of *Selected Topics in Solid State Physics* (North-Holland, New York, 1981) p. 120.

[11]D. K. Wagner and R. Bowers, Adv. Phys. **27**, 651 (1978).

[12]T. Wegehaupt and R. E. Doezma, Phys. Rev. B **18**, 742 (1978).

[13]V. F. Gantmakher, Rep. Prog. Phys. **37**, 317 (1974).

[14]V. F. Gantmakher and Yu. S. Leonev, Pis'ma Zh. Eksp. Teor. Fiz. **8**, 162 (1968) [JETP Lett. **8**, 162 (1968)].

[15]V. F. Gantmakher and V. T. Dolgopolov, Zh. Eksp. Teor. Fiz. **60**, 2260 (1971) [Sov. Phys.—JETP **33**, 1215 (1971)].

[16]A. Myers, R. S. Thompson, and Z. Ali, J. Phys. F **4**, 1707 (1974).

[17]A. B. Meador and W. E. Lawrence, Phys. Rev. B **15**, 1850 (1977).

[18]N. W. Ashcroft and W. E. Lawrence, Phys. Rev. **175**, 938 (1968).

[19]D. G. Garrett and J. C. Swihart, J. Phys. F **6**, 1781 (1976).

[20]J. C. Swihart, D. G. Garrett, and B. K. Bhattacharyya, Phys. Lett. **85A**, 295 (1981).

[21]C. J. P. M. Harmans, thesis, Free University, Amsterdam, 1975.

[22]P. M. Holtham, J. Phys. F **6**, 1457 (1976).

[23]A. J. Hughes and J. P. G. Sheperd, J. Phys. C **2**, 661 (1969).